Research Article | Vol. 9, No. 11 | 1 Nov 2018 | BIOMEDICAL OPTICS EXPRESS 5296
Biomedical Optics EXPRESS

Directional changes in information flow between human brain cortical regions after application of anodal transcranial direct current stimulation (tDCS) over Broca's area

JIANWEI CAO, XINLONG WANG, HANLI LIU, AND GEORGE ALEXANDRAKIS*

University of Texas at Arlington & University of Texas Southwestern Medical Center at Dallas, Joint Graduate Program in Biomedical Engineering, Arlington, Texas 76010
**galex@uta.edu*

Abstract: Little work has been done on the information flow in functional brain imaging and none so far in fNIRS. In this work, alterations in the directionality of net information flow induced by a short-duration, low-current (2 min 40 s; 0.5 mA) and a longer-duration, high-current (8 min; 1 mA) anodal tDCS applied over the Broca's area of the dominant language hemisphere were studied by fNIRS. The tDCS-induced patterns of information flow, quantified by a novel directed phase transfer entropy (dPTE) analysis, were distinct for different hemodynamic frequency bands and were qualitatively similar between low and high-current tDCS. In the endothelial band (0.003–0.02 Hz), the stimulated Broca's area became the strongest hub of outgoing information flow, whereas in the neurogenic band (0.02–0.04 Hz) the contralateral homologous area became the strongest information outflow source. In the myogenic band (0.04–0.15 Hz), only global patterns were seen, independent of tDCS stimulation that were interpreted as Mayer waves. These findings showcase dPTE analysis in fNIRS as a novel, complementary tool for studying cortical activity reorganization after an intervention.

1. Introduction

Transcranial direct current stimulation (tDCS) is a non-invasive electrical stimulation technique used to modulate cortical activity in the human brain by delivering weak currents through a pair of anode-cathode electrodes (up to 2mA for up to 20 mins) [1,2]. TDCS has been applied to enhance physical performance in healthy subjects [3–5] and facilitate neurorehabilitation during stroke recovery [6]. Several studies have suggested that anodal tDCS over either Broca's area or Wernicke's area could improve naming accuracy or speed both in stroke-induced aphasia patients [7–9] and in healthy subjects [5,10,11].

Recent resting-state functional magnetic resonance imaging (fMRI) studies [12,13] explored the altered connectivity strength within large-scale functional networks related to tDCS stimulation over language cortical regions. However, little is known about the directionality of cortical interactions in functional language networks when tDCS is applied. To the best of our knowledge, only one study [14] to date has investigated the direction of information flow, which was done by use of Dynamic Causal Modelling (DCM) during a concurrent tDCS-fMRI study of overt picture naming. Nevertheless, DCM requires complicated *a priori* parameters and strong assumptions on the underlying neuronal interaction mechanisms [15,16]. Here, we used Phase Transfer Entropy (PTE) [15,17], which is a computationally efficient and data-driven method, to estimate changes in the direction of information flow affected by tDCS, quantified by a directional PTE (dPTE) metric.

In this study we used functional near-infrared spectroscopy (fNIRS) to investigate directionality in cortical interactions involving the language processing areas. FNIRS can detect changes in the concentration of oxyhemoglobin (ΔHbO) and deoxyhemoglobin (ΔHb)

#335421 https://doi.org/10.1364/BOE.9.005296
Journal © 2018 Received 18 Jun 2018; revised 14 Sep 2018; accepted 2 Oct 2018; published 10 Oct 2018

Biomedical Optics EXPRESS

resulting from neurovascular coupling secondary to neuronal activation [18]. The higher temporal resolution of fNIRS and its easier implementation in a compatible setup with tDCS, relative to fMRI, makes it advantageous for studying alterations in functional connectivity induced during tDCS [19,20]. Previous studies [21,22] have shown that vasomotion-induced oscillations measured by fNIRS, which lead to improved perfusion [23] and local tissue oxygenation [24], could be divided into three frequency bands: an endothelial component (0.003-0.02Hz) related to microvascular activity [25–27], a neurogenic component (0.02-0.04Hz) linked to intrinsic neuronal activity [28] and a myogenic component (0.04-0.15Hz) attributed to the activity of smooth muscles of arterioles [25–27]. In this study, we explored how tDCS affected the directionality of information flow, encoded by changes in dPTE, in these three individual frequency bands and in the entire fNIRS frequency band.

One additional aspect we explored in this work was the effect of tDCS current intensity on the information flow patterns of language-processing networks. A subdivision of information flow analysis into endothelial, neurogenic and myogenic frequency band contributions to the information flow computed by dPTE analysis was performed with the aim of helping clarify the relative roles of neuronal versus vascular physiological responses to different tDCS current intensities. Furthermore, we wanted to evaluate whether alterations of information flow due to anodal tDCS over the left Broca's area for a brief duration (2 min 40 s) and low intensity tDCS current (0.5 mA), henceforth referred to as Low Current tDCS, could produce qualitatively similar information flow directionality patterns to those occurring after a longer duration (8 min) and higher intensity tDCS current (1 mA), henceforth referred to as High Current tDCS, mimicking a common intervention choice in the literature. The aim of this latter part of the work was to test whether Low Current tDCS, whose hemodynamic effects wash away within minutes, could be used as a rapid way to produce qualitatively similar cortical maps of information flow directionality as those occurring at therapeutic level currents, which have long-lasting effects. The findings of this work are intended to contribute towards a better understanding of cortical plasticity in language networks induced by tDCS.

2. Method and materials

2.1 Subjects

Thirteen healthy right-handed subjects (2 Females, 11 Males, mean ± SD age = 35.4 ± 8.4) participated in this study. Subject handedness was determined by the Edinburgh Handedness Inventory [29]. None of them had a history of neurological disorders. Written informed consent was obtained from each participant before the experiments. The studies were conducted under the approval of the University of Texas at Arlington Institutional Review Board protocol (UTA #2015-0819).

2.2 fNIRS imaging setup combined with tDCS

Figure 1(a) demonstrates the overall experimental setup. A continuous-wave fNIRS imaging system (LABNIRS, Shimadzu, Japan) was used to collect signals. Figure 1(b) illustrates the fNIRS source-detector geometry, which consisted of 26 sources and 28 detectors with a separation of 3 cm, resulting in 83 source-detector channels. The optical fiber bundles of sources and detectors were inserted into the optode holder on the subject's head. Light was emitted at wavelengths of 780nm, 805nm, and 830nm simultaneously from each source. FNIRS signals were sampled at a frequency of 12.35 Hz. This probe geometry covered language-related cortical regions, including the Broca's and Wernicke's areas as well as some prefrontal cortical regions including the frontopolar, dorsolateral prefrontal cortex (DPFLC) and premotor areas, all for both hemispheres.

A co-registration procedure was applied to measure the covered cortical regions based on cranial landmark measurements on all the subjects [30]. Five reference cranial landmarks (nasion, inion, left and right preauricular points and vertex) and the locations of all source and

Biomedical Optics EXPRESS

detector optodes were measured by a motion tracking system (Fastrak, POLHEMUS). NIRS-SPM [31] was used to calculate the Montreal Neurological Institute (MNI) coordinates of the optodes [32] and register them on a standard MRI brain template [33] to identify the Brodmann areas (BAs) imaged by each source-detector channel. The layout of spatially registered channels (averaged over all thirteen subjects) on the standard human brain atlas is shown in Fig. 2.

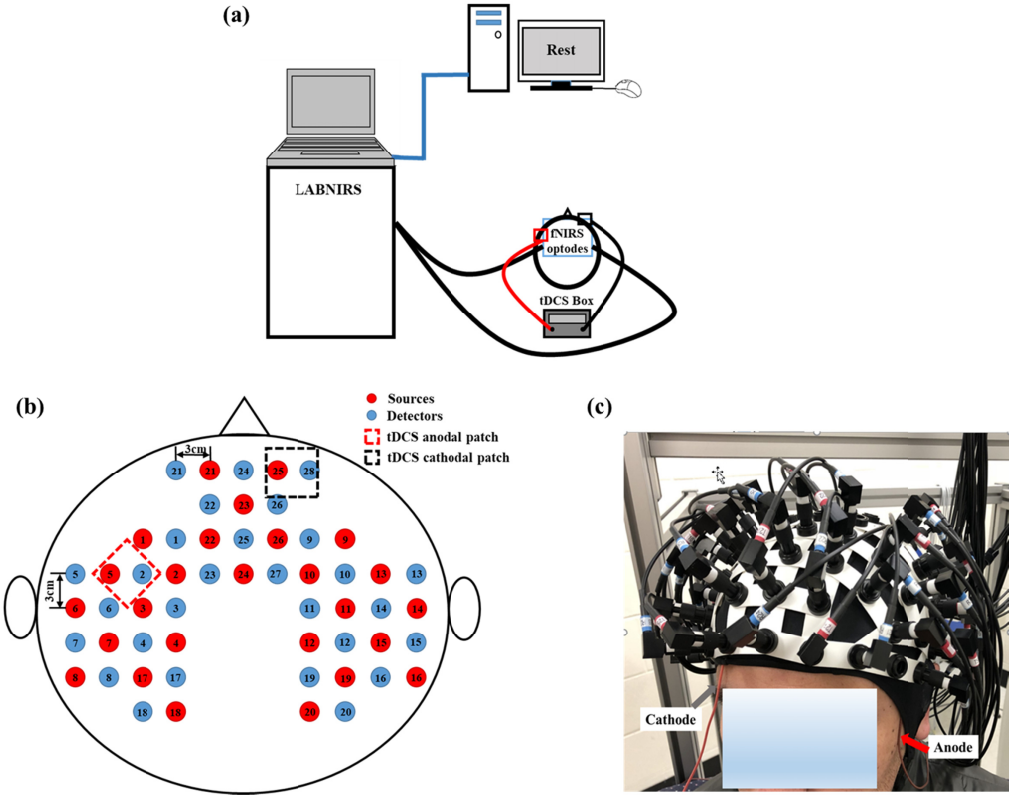

Fig. 1. (a) Overall experimental setup. The computer screen only displays the word "Rest" during data acquisition. FNIRS optodes and tDCS electrodes were placed on the subject's head as described in "FNIRS Imaging Setup Combined with tDCS". (b) The fNIRS probe geometry with 26 sources and 28 detectors placed over a subject's head. The separation of all source and detectors was 3 cm. (Red dots: sources, Blue dots: detectors). (c) Placement of fNIRS-tDCS assembly on a subject's head. The gray arrow points to the wire connecting the cathodal patch and the red arrow points to the wire connecting the anodal patch.

Biomedical Optics EXPRESS

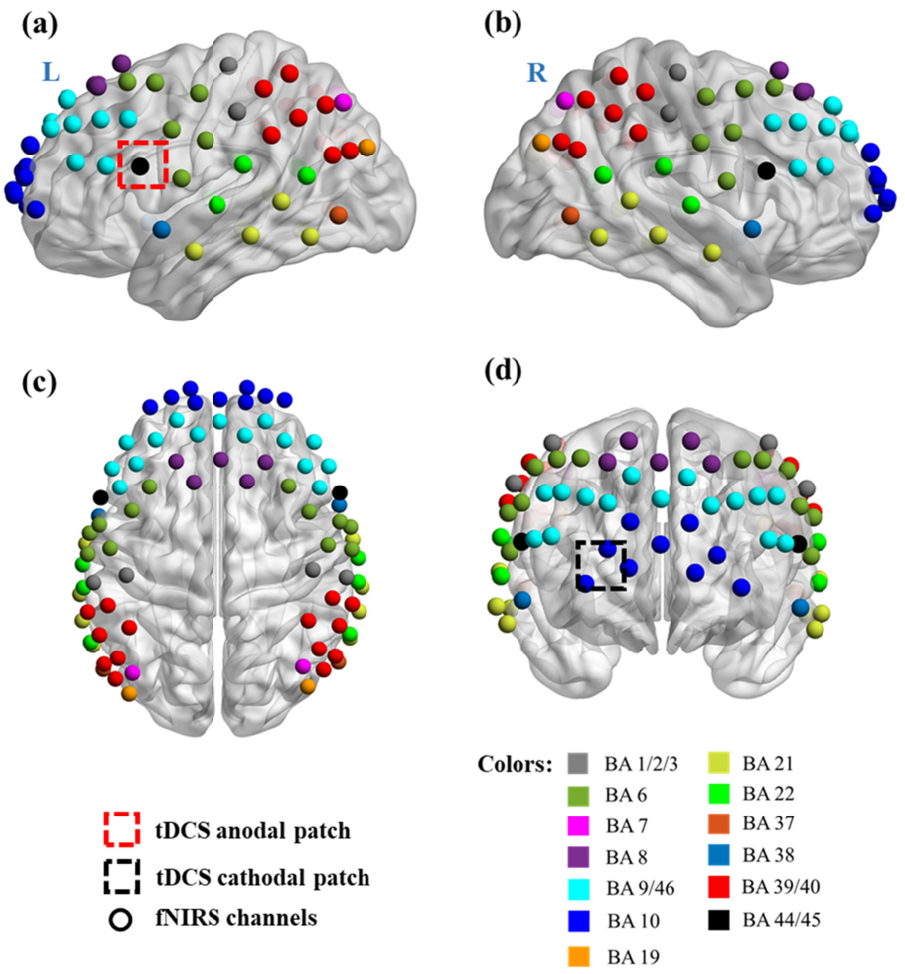

Fig. 2. Co-registration of fNIRS source-detector channels (mid-way points between source and detector pairs) on a standard human brain atlas: (a) Sagittal view (Left), (b) Sagittal view (Right), (c) Top view and (d) Coronal view. The tDCS anodal (red dashed square) and cathodal (black dashed square) patches were placed on the left FC5 position, shown in (a), and the right Fp2 position, shown in (d), respectively.

TDCS current was delivered by a battery-driven electrical stimulator (Phoresor II, IOMED Inc., Salt Lake City, UT) through a pair of saline-soaked gauze covered gel electrodes (5 × 5 cm; IOMED Inc., Salt Lake City, Utah). The placement of tDCS patches used the EEG International 10/20 system [34] as a reference, with the anodal patch placed over the FC5 position (centered at Channel 27 in our setup) to stimulate left Broca's area, and the cathodal patch centered over the Fp2 position [11] as a control location [dashed square in Figs. 2(a)-2(d)]. In order to accommodate optical fiber bundles overlapped spatially with the patches, two 0.5 cm-diameter holes were punctured on each patch.

2.3 Protocol design

During fNIRS measurements, subjects were asked to keep at rest with their eyes closed but staying awake for 32 minutes. Figure 3 illustrates the timeline of the protocol. There were four stimulation sessions: (1) Before tDCS (0-6 min) was the first 6 minutes without tDCS applied, which was regarded as the baseline measurement. (2) Low Current tDCS (6-14 min), which entailed 0.5 mA current tDCS being applied for 2 min 40 s, followed by a no-

stimulation period of 5 min and 20 s to allow any hemodynamic changes incurred by Low Current tDCS to go back to baseline [1,35,36]. (3) High Current tDCS (14-22 min), which entailed a higher current of 1 mA being applied for 8 min [1]. (4) After High Current tDCS (22-32 min), which was the 10 min period immediately after High Current tDCS. Subjects were not told when tDCS was being applied.

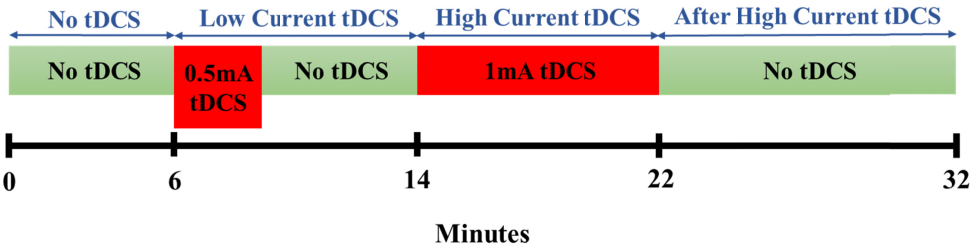

Fig. 3. The tDCS protocol timeline.

2.4 Data preprocessing

This study used the publically available Homer toolbox [37] to process the acquired time-series fNIRS data. Firstly, the data from each channel was band-pass filtered: 0.003-0.15Hz to isolate the entire range of physiologically relevant hemodynamic fluctuations, 0.003-0.02 Hz for endothelial origin fluctuations, 0.02-0.04 Hz for neurogenic origin fluctuations and 0.04-0.15 Hz for myogenic origin fluctuations [21,22,38]. Subsequently, global fluctuations that were detected across all channels were removed by principal component analysis (PCA) [39,40]. Data was further de-noised by removing source-detector pair measurement channels that had signal standard deviations greater than two times their mean signal amplitude [41]. About 5% of the measurement channels were removed. Changes in hemoglobin concentration relative to the baseline (ΔHbO) were then quantified by a modified Beer-Lambert Law [42]. Correlation-based signal improvement (CBSI) [43] was adopted to remove motion artifacts based on negative correlations between oxygenated and deoxygenated hemoglobin dynamics.

2.5 Phase transfer entropy (PTE) and directed PTE (dPTE) data analysis

PTE estimates the information flow between regions of interest (ROIs) based on the same principle as Wiener-Granger Causality [15,17]. It is calculated as the difference between the uncertainty of the target signal Y conditioned only on its own past and the uncertainty of the target signal conditioned on both the past of its own and the source signal X [17]:

$$PTE_{xy} = H\left(Y_{t+\delta}|Y_t\right) - H\left(Y_{t+\delta}|Y_t, X_t\right), \tag{1}$$

where PTE_{xy} denotes the phase transfer entropy from X to Y, H represent the entropy, δ denotes the time delay. If PTE_{xy} is larger than zero, then the source signal X has a causal influence on the target signal Y. Since PTE_{xy} lacks a meaningful upper bound, a normalization process is utilized to reduce biases [44,45]:

$$dPTE_{xy} = \frac{PTE_{xy}}{PTE_{xy} + PTE_{yx}}, \tag{2}$$

If $0.5 < dPTE_{xy} \le 1$, the information flow is preferentially from X to Y. If $0 \le dPTE_{xy} < 0.5$, the information flow is preferentially from Y to X. If $dPTE_{xy} = 0.5$, there is no preferential information flow between X and Y.

Biomedical Optics EXPRESS

2.6 Data processing steps for dPTE analysis

DPTE analysis was applied to calculate information flow for the entire physiologically relevant range of hemodynamic fluctuation frequencies, and the individual endothelial, neurogenic and myogenic frequency bands for the four stimulation sessions described above (Before tDCS, Low Current tDCS, High Current tDCS and After High Current tDCS). Specifically, for each subject, PTE analysis was performed to determine the causality between every two channels among all 83 channels. Then PTE values were normalized into dPTE values. This generated a 83 × 83 dPTE matrix determining information flow between all channel pairs. The value at Xth row and Yth column determined the scale of information flow from Y to X. Then dPTE was averaged along rows to produce a 1 × 83 matrix, which was the mean dPTE between each one channel and all other channels. If the mean dPTE of one channel was >0.5, then the average information flow between this channel and all the other channels was outgoing. If the mean dPTE of one channel was <0.5, then the average information flow was incoming. The group-averaged mean dPTE was calculated by averaging the mean dPTE by subject. The above procedures were repeated for all hemodynamic frequency bands for each of the four stimulation sessions. Next, a set of paired t-tests among the 13 subjects was performed on dPTE between the four stimulation sessions for each frequency band. Significant enhancements of information flow ($p<0.05$) from selected seeds, i.e. the left stimulated Broca's area and the right contralateral Broca's homologue, were identified. Lastly, the group-averaged mean dPTE values for each channel were interpolated on a standard MRI brain template by EasyTopo software [46], and the significant changes in information flow from selected seeds were displayed topographically on the standard MRI brain template by BrainNet View software [47].

3. Results

3.1 Direction of information flow in the entire fNIRS frequency band (0.003–0.15 Hz)

Figure 4 shows the map of average information flow between each channel and all other channels over the cortical regions being mapped by fNIRS by use of dPTE analysis for the four stimulation sessions (Before tDCS, Low Current tDCS, High Current tDCS and After High Current tDCS). The color-coded map illustrates a single estimate of net direction of information flow (outgoing or incoming) for each channel. Figures 4(a)-4(d) show top views, Figs. 4(e)-4(h) lateral left views, Figs. 4(i)-4(l) lateral right views and Figs. 4(m)-4(p) frontal views. Figures 4(f)-4(h) show that, compared to the Before tDCS session, the stimulated left Broca's area (BA44/45) indicated by black circles became an outgoing information flow hot spot during Low Current tDCS, High Current tDCS and After High Current tDCS. In addition, the left middle temporal gyrus (MTG, BA 21) indicated by a pink circle in Fig. 4(g) became an additional hot spot of outgoing information only during High Current tDCS. Figures 4(j)-4(l) illustrate the cortical areas contralateral to the stimulated hemisphere, including right Broca's homologue (BA44/45), superior temporal gyrus (STG, BA22) and MTG (BA21) collectively circumscribed by blue ovals, that also became hot spots of outgoing information during Low Current tDCS, High Current tDCS and After High Current tDCS. Overall, tDCS stimulation induced an increase in outgoing information both from the stimulated area and the contralateral hemisphere region that was distant from the anodal stimulation patch, as noted by the higher dPTE values over these areas in Fig. 4. Individual subject dPTE maps for the entire fNIRS frequency band are also shown in the Appendix, Fig. 10 for the subset of dPTE views including the stimulated Broca's area. Though individual variations are seen, not unlike to what is typically observed in activation images, the stimulated Broca's area is consistently identifiable as a dPTE source post-stimulation. The cortical locations of fNIRS channels receiving the information emanating from individual seed fNIRS channels located near the center of the hot spots identified in this section were analyzed next.

Biomedical Optics EXPRESS

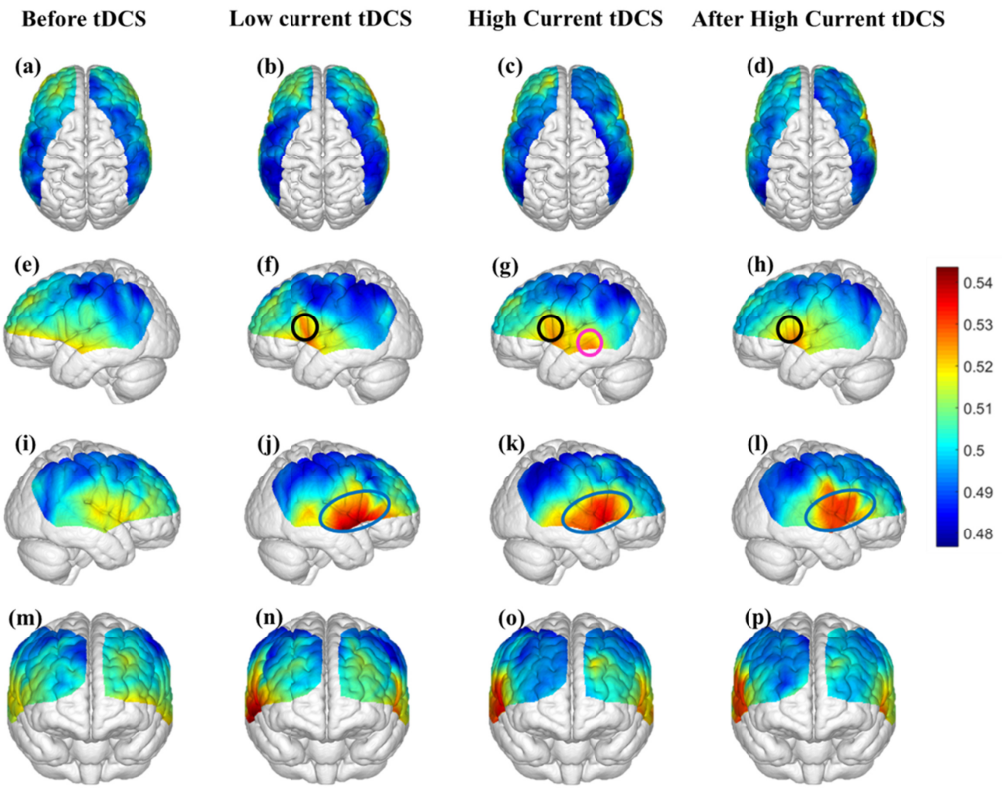

Fig. 4. Mean dPTE for each channel displayed as a color-coded map viewed from top, left, right and front for the four stimulation sessions: Before tDCS [(a), (e), (i) and (m)], Low Current tDCS [(b), (f), (j) and (n)], High Current tDCS [(c), (g), (k) and (o)] and After High Current tDCS [(d), (h), (l) and (p)]. Hot (yellow – red) and cold (blue – green) colors indicate information outflow and inflow, respectively.

3.2 Information flow using the stimulated left Broca's area as the seed

The channel near the center of the stimulated left Broca's area, indicated by a black circle in Figs. 4(f)-4(h), was chosen as the seed to compute the outgoing information patterns for all stimulation sessions. Figure 5 shows the channel locations over cortical areas with significant changes in information flow direction between the Before tDCS session versus each one of the other three stimulation sessions (Low Current tDCS, High Current tDCS and After High Current tDCS), as deduced from paired t-tests. Figures 5(a)-5(c) show lateral left views and Figs. 5(d)-5(f) show top views. Only enhanced efflux of information from the left Broca's area was observed for each comparison condition. Table 1 lists the Brodmann areas with significantly increased outgoing information emanating from the left Broca's area for the three stimulation sessions compared to Before tDCS. It is noteworthy that High Current tDCS brought about a significant increase in information flowing into the left MTG (BA 21), as seen in Fig. 5(b), which was also a hot spot for outgoing information during High Current tDCS as indicated by the area in the pink circle in Fig. 4(g).

Biomedical Optics EXPRESS

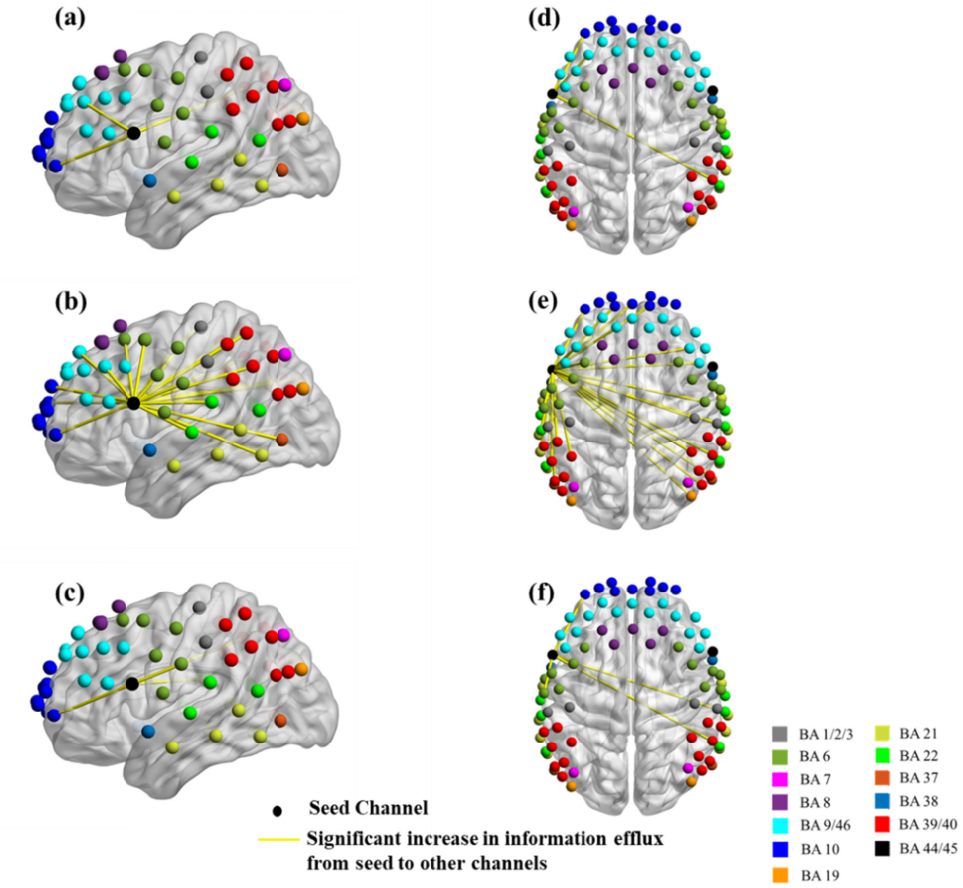

Fig. 5. Changes in information flow direction between the left Broca's area (seed) and other cortical regions induced by different tDCS stimulation conditions. Group-level significant differences ($p<0.05$) in information flow direction between pairs of detector locations for Before tDCS versus Low Current tDCS [(a), (d)], versus High Current tDCS [(b), (e)], and versus After High Current tDCS [(c), (f)].

Table 1. Brodmann areas with significantly increased information influx originating from Channel 27 (left Broca's area)

Seed: Channel 27	Low Current tDCS	High Current tDCS	After High Current tDCS
Ipsilateral Hemisphere			
Brodmann Area 6		Yes	Yes
Brodmann Area 9	Yes	Yes	
Brodmann Area 10	Yes	Yes	Yes
Brodmann Area 21		Yes	
Brodmann Area 22/39/40		Yes	
Contralateral Hemisphere			
Brodmann Area 6		Yes	
Brodmann Area 9		Yes	
Brodmann Area 10		Yes	
Brodmann Area 22/39/40	Yes	Yes	Yes

BA 6: Premotor Area; BA 9: Dorsolateral Prefrontal Cortex; BA 10: Frontopolar Area; BA 21: Middle Temporal Gyrus (MTG); BA 22/39/40: Wernicke's area.

Also, the left MTG, which was an outgoing information flow hot spot for High Current tDCS, showed enhanced information flow into the frontopolar (BA 10), DLPFC (BA 9), premotor (BA 6) and Wernicke's (BA 22/39/40) areas for both hemispheres. Due to the

Biomedical Optics EXPRESS

similarity of these findings to the case where the left Broca's area was the seed, we do not show these results for brevity.

3.3 Information flow using the contralateral right Broca's homologue as the seed

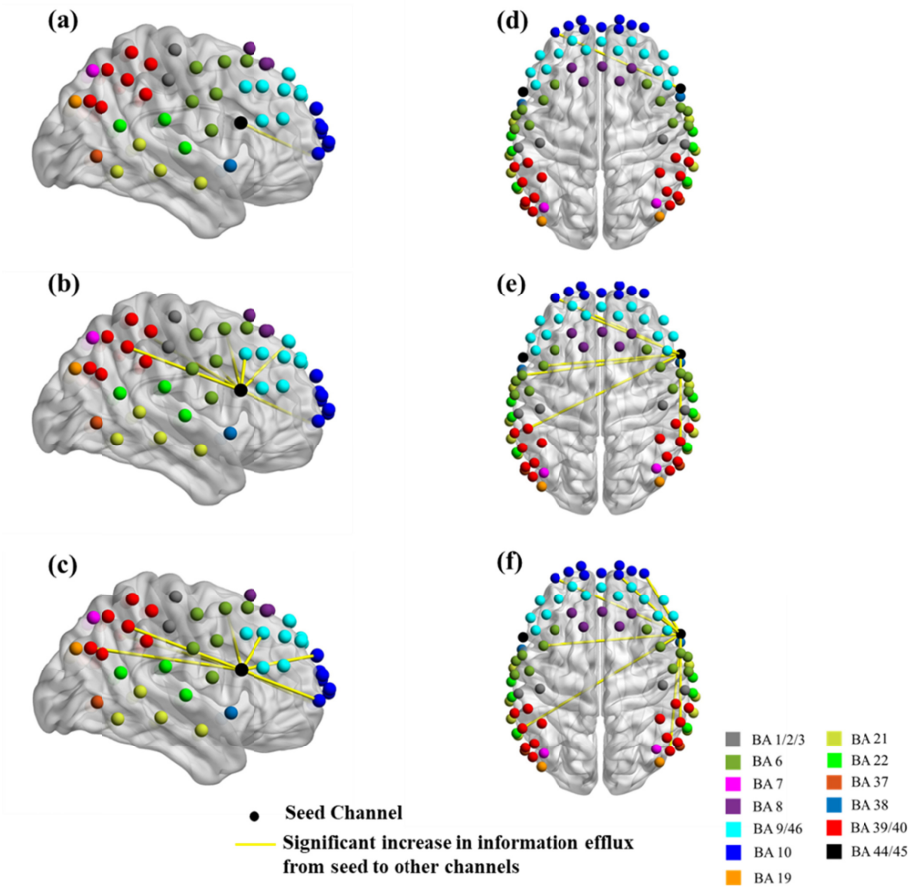

Fig. 6. Changes in information flow direction between the right Broca's homologue (seed) and other cortical regions induced by different tDCS stimulation conditions. Group-level significant differences ($p<0.05$) in information flow direction between pairs of detector locations for Before tDCS versus Low Current tDCS [(a), (d)], versus High Current tDCS [(b), (e)], and versus After High Current tDCS [(c), (f)].

The right Broca's homologue contralateral to the stimulated region, included within the blue ovals in Figs. 4(j)-4(l), was also studied for changes in information flow patterns as was done for the stimulated left Broca's area above. Figure 6 shows channel locations over cortical areas with significant changes in information flow direction using the contralateral Broca's homologue as the seed. These information flow direction changes were deduced from paired t-tests between Before tDCS versus each one of the other stimulation sessions. Several qualitative similarities were observed in the information flow direction changes when comparing to the corresponding results from the stimulated left Broca's area: (1) Only enhanced efflux of information from the right Broca's homologue was observed for each stimulation condition, and (2) The dPTE information flow values were higher towards other cortical regions for High Current tDCS compared to Low Current tDCS. However, in contrast to the case of the left Broca's area as the seed, dPTE information flow persisted at higher values for the After High Current tDCS condition compared to Low Current tDCS. Table 2 lists the Brodmann areas with significantly increased outgoing information from the right

Biomedical Optics EXPRESS

Broca's homologue for the three stimulation conditions compared to the Before tDCS condition.

Table 2. Brodmann areas with significantly increased information influx originating from Channel 34 (right Broca's homologue)

Seed: Channel 34	Low Current tDCS	High Current tDCS	After High Current tDCS
Ipsilateral Hemisphere			
Brodmann Area 9		Yes	Yes
Brodmann Area 10			Yes
Brodmann Area 22/39/40		Yes	Yes
Contralateral Hemisphere			
Brodmann Area 6		Yes	Yes
Brodmann Area 9		Yes	
Brodmann Area 10	Yes	Yes	Yes
Brodmann Area 22/39/40		Yes	Yes

BA 6: Premotor Area; BA 9: Dorsolateral Prefrontal Cortex; BA 10: Frontopolar Area; BA 22/39/40: Wernicke's area.

3.4 Information flow in the endothelial frequency band (0.003–0.02 Hz)

Figure 7 shows the average information flow in the endothelial frequency band between any channel location and all other cortical regions by using dPTE analysis for four different sessions (Before tDCS, Low Current tDCS, High Current tDCS and After High Current tDCS). The color-coded map illustrates a single estimate of preferred direction of information flow (outgoing or incoming) for each channel.

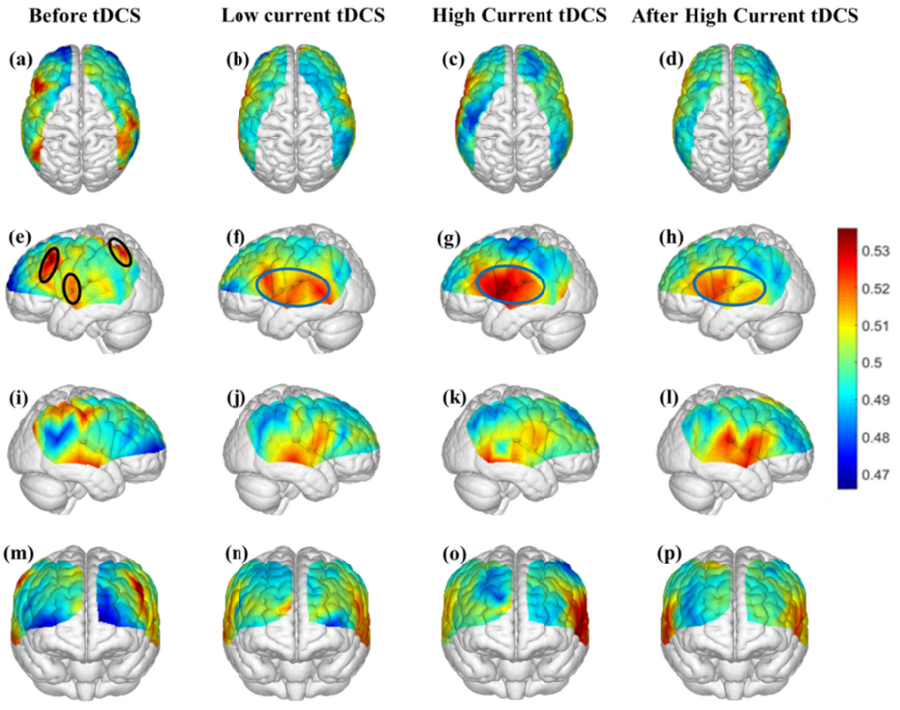

Fig. 7. Mean dPTE in the endothelial frequency band for each channel displayed as a color-coded map viewed from top, left, right and front for four different sessions: Before tDCS [(a), (e), (i) and (m)], Low Current tDCS [(b), (e), (j) and (n)], High Current tDCS [(c), (g), (k) and (o)] and After High Current tDCS [(d),(h), (l) and (p)]. Hot (yellow – red) and cold (blue – green) colors indicate information outflow and inflow, respectively.

Figure 7(e) shows that during the initial Before tDCS session the outgoing information was generated from the DLPFC (BA 9), MTG (BA 21) and Somatosensory Association

Biomedical Optics EXPRESS

Cortex (BA 7) regions indicated by black ovals, which are part of the default model network (DMN) [48]. In contrast, during and after stimulation the Broca's area (BA 44/45), MTG (BA21) and STG (BA 22), all circumscribed within a blue oval in Figs. 7(f)-7(h) became the hot spots for outgoing information. In addition, in the non-stimulated contralateral hemisphere, shown in Figs. 7(i)-7(l), dPTE increases were seen in the vicinity of the contralateral right Broca's homologue for the endothelial frequency band during all stimulation sessions.

Subsequently, the Broca's area, MTG and STG hot spots in the left hemisphere were chosen as the seeds for determining where the outgoing information was directed out of these regions on the cortex. Only Brodmann areas with significant increases in outgoing information from all the seeds, compared to Before tDCS, were illustrated in Table 3. For Low Current tDCS and After High Current tDCS, increased information flow was directed into the same Brodmann areas, while for High Current tDCS, increased information flow occurred into additional cortical regions, which are also part of the language-processing network [49–51].

Table 3. Brodmann areas with significantly increased information influx originating from hot spots in the left hemisphere

Hot spots on left hemisphere	Low Current tDCS	High Current tDCS	After High Current tDCS
Ipsilateral Hemisphere			
Brodmann Area 6		Yes	
Brodmann Area 9		Yes	
Brodmann Area 40	Yes	Yes	Yes
Contralateral Hemisphere			
Brodmann Area 40	Yes	Yes	Yes

Hot spots: Left Broca's area, MTG and STG. BA 6: Premotor Area; BA 9: Dorsolateral Prefrontal Cortex; BA 10: Frontopolar Area; BA 22/39/40: Wernicke's area.

3.5 Information flow in the neurogenic frequency band (0.02–0.04 Hz)

Figure 8 shows information flow in the neurogenic frequency band between any channel location and all other cortical regions by applying dPTE analysis to each of the four sessions (Before tDCS, Low Current tDCS, High Current tDCS and After High Current tDCS). The color-coded map illustrates a single estimate of direction of information flow (outgoing or incoming) for each channel. Figure 8(i) shows that during the initial Before tDCS session the outgoing information hot spots were located over the DPFLC (BA 9), indicated by black ovals, which is part of the DMN [48]. In contrast, during and after stimulation the hot spots shifted to the Broca's area (BA 44/45), MTG (BA21) and STG (BA 22) of the left hemisphere, indicated by blue ovals in Figs. 8(j)-8(l). It is noteworthy that when comparing to the left hemisphere, Figs. 8(e)-8(h), where the anodal stimulation over Borca's area was applied, it appears that higher changes in dPTE occurred in the right hemisphere for the neurogenic frequency band. It is suspected that these information flow changes occurring in the hemisphere contralateral to the stimulation were facilitated by interhemispheric connections through the corpus callosum [52].

Biomedical Optics EXPRESS

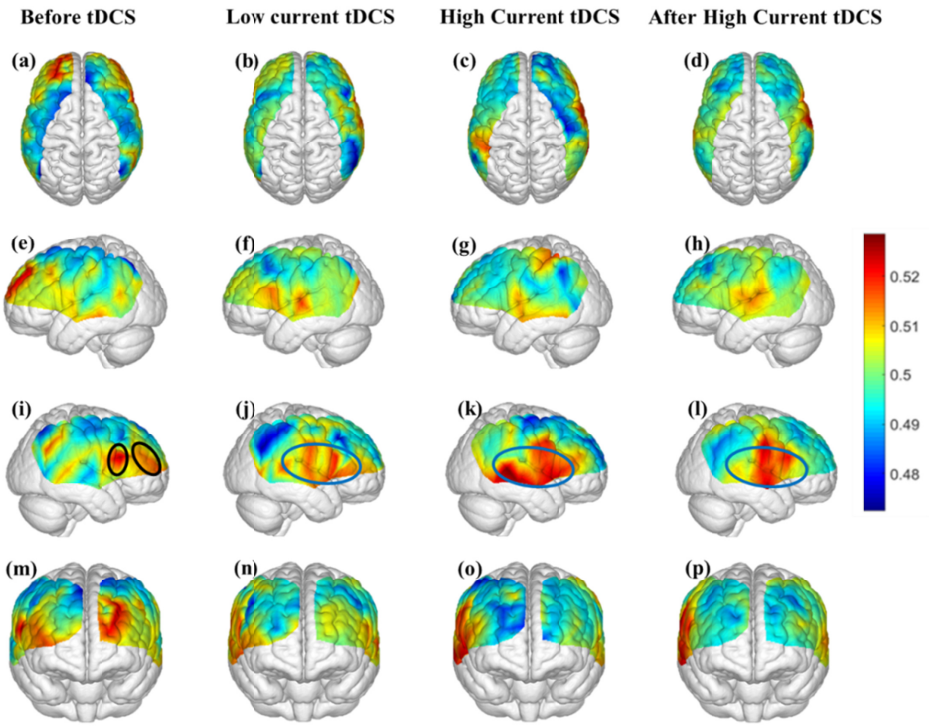

Fig. 8. Mean dPTE in the neurogenic frequency band for each channel displayed as a color-coded map viewed from top, left, right and front for four different sessions: Before tDCS [(a), (e), (i) and (m)], Low Current tDCS [(b), (f), (j) and (n)], High Current tDCS [(c), (g), (k) and (o)] and After High Current tDCS [(d),(h), (l) and (p)]. Hot (yellow – red) and cold (blue – green) colors indicate information outflow and inflow, respectively.

Subsequently, the Broca's area, MTG and STG hot spots in the right hemisphere were chosen as the seeds for determining where the outgoing information was directed from these regions to other cortical areas. Only Brodmann areas with significant increases in outgoing information from all these seed regions, compared to Before tDCS, were illustrated in Table 4. Interestingly, in contrast to the results for the endothelial frequency band shown in Table 3, enhanced information flow occurred towards a larger number of cortical regions, corresponding to Brodmann areas listed in Table 4, during High Current tDCS. The higher information outflow effect over these Brodmann areas persisted during the After High Current tDCS condition. The longevity of these information flow patterns beyond the current stimulation period hints at the possibility that these effects are tDCS-induced changes in neuronal activity, possibly mediated by long-term potentiation (LTP) [53–55].

Table 4. Brodmann areas with significantly increased information influx originating from hot spots in the right hemisphere

Hot spots on right hemisphere	Low Current tDCS	High Current tDCS	After High Current tDCS
Ipsilateral Hemisphere			
Brodmann Area 9		Yes	Yes
Brodmann Area 10		Yes	Yes
Brodmann Area 40	Yes	Yes	Yes
Contralateral Hemisphere			
Brodmann Area 6		Yes	Yes
Brodmann Area 40	Yes	Yes	Yes

Hot spots: Right Broca's homologue, MTG and STG. BA 6: Premotor Area; BA 9: Dorsolateral Prefrontal Cortex; BA 10: Frontopolar Area; BA 22/39/40: Wernicke's area.

Biomedical Optics EXPRESS

3.6 Information flow in the myogenic frequency band (0.04–0.15 Hz)

Figure 9 shows information flow in the myogenic frequency band between any channel location and all other cortical regions by applying dPTE analysis to each of the four sessions (Before tDCS, Low Current tDCS, High Current tDCS and After High Current tDCS), as was done above for the other frequency bands. Figures 9(m)-9(p) show that for all four stimulation sessions, the hot spots of outgoing information appeared in the frontopolar areas (BA 10) of both hemispheres, indicated by black ovals. No significant change was found in the PTE of hot spots of each hemisphere between stimulation sessions. Therefore, information outflow in these hot spots was not affected by the stimulation. The dPTE in key language areas (Broca's area and Wernicke's area) were not affected by stimulation either. Therefore, we did not pursue any further seed-based analysis for this frequency band as was done for the endothelial and neurogenic bands.

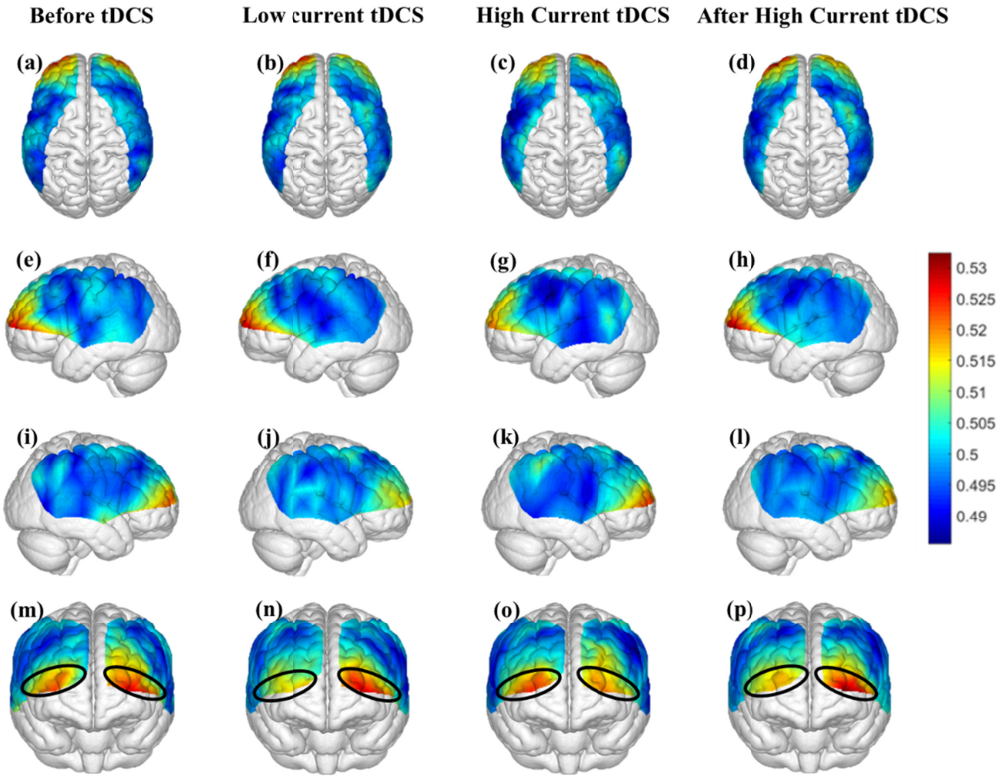

Fig. 9. Mean dPTE in the myogenic frequency band for each channel displayed as a color-coded map viewed from top, left, right and front for four different sessions: Before tDCS [(a), (e), (i) and (m)], Low Current tDCS [(b), (f), (j) and (n)], High Current tDCS [(c), (g), (k) and (o)] and After High Current tDCS [(d),(h), (l) and (p)]. Hot (yellow – red) and cold (blue – green) colors indicate information outflow and inflow, respectively.

3.7 Quantification of dPTE source and sink patterns

The spatial extent of net information flow sources and sinks, as defined by dPTE values (dPTE< 0.5, sink; dPTE> 0.5, source) [[44,45]], was calculated for the maps shown in Figs. 4, 7 and 8 for all hemodynamic frequency bands, and the endothelial and neurogenic bands, respectively. No such analysis was done for the myogenic band since it was invariant to stimulation. The resulting number of fNIRS channels acting as sources or sinks per BA were quantified for each subject and stimulation session (Before tDCS, Low Current tDCS, High Current tDCS, After High Current tDCS). Subsequently, paired t-tests were performed

Biomedical Optics EXPRESS

between Before tDCS and each one of the other stimulation conditions for all fNIRS channels belonging to each BA. Interestingly, we found that the number of fNIRS channels mapping the stimulated Broca's area and the associated language processing cortical regions (STG – BA 44/45, MTG – BA 21, STG – BA 22, and contralateral Broca's homologue – BA 44/45) retained their identity as sources or sinks between stimulation conditions. The only thing that changed was that, on average, their dPTE weight increased for all stimulation conditions, compared to baseline. Nevertheless, the number of channels mapping these regions did not show statistically significant differences between pre- and post-stimulation. It is therefore concluded that the size of sources related to language processing areas did not change significantly with tDCS, at least within the spatial sampling limits of our fNIRS setup. However, the average value of dPTE outflow increased (Before tDCS versus Low Current tDCS, $p=0.043$; Before tDCS versus High Current tDCS, $p<0.001$; Before tDCS versus After High Current tDCS, $p=0.031$). In contrast, the dPTE patterns of some cortical regions that are part of the DMN [48] (DLPFC – BA 9 and Somatosensory Association Cortex – BA 7) and not overlapping with language-processing BAs changed from sources before stimulation to sinks after stimulation.

4. Discussion

This study explored the impact of anodal tDCS applied over the left Broca's area on the direction of information flow deduced from hemodynamic fluctuations in the fNIRS signal as a whole and in three distinct frequency sub-bands that are known to be attributed to endothelial, neurogenic and myogenic activity. Despite the lower spatial resolution and tissue depth probed compared to fMRI, the higher temporal resolution of fNIRS and its ability to easily collect data during electrical stimulation has enabled us to demonstrate different patterns of information flow induced by tDCS for different frequency bands.

4.1 dPTE analysis of all fNIRS frequencies (0.003-0.15 Hz)

Anodal stimulation over the left Broca's area made not only that region, but also its non-stimulated counterpart in the contralateral hemisphere strong emitters of information flow towards other language-processing areas. This is evident in the Fig. 4 hot spots for the three tDCS stimulation conditions, where the cold spots are the cortical areas of reception of information efflux from the hot spots. These results are consistent with a prior EEG study where TMS was applied alternately over the left and right anterior temporal lobes, and the left and right superior parietal lobes [56]. That study found that TMS applied on all four stimulation sites evoked a consistent increase of information flow around the stimulation site and its contralateral cortical region in the broad EEG frequency band of 3-45Hz. That study reported that the direction of stimulation affects cortical areas with established neuronal connections through two main commissural fibers [57].

The effect of stimulation on information flow across both hemispheres is shown in Table 1 and Table 2 that identify the cortical areas receiving information from the left Broca's area and its homologue, respectively. For the ipsilateral hemisphere to the stimulation, those cortical areas are not only structurally connected with Broca's area through white matter tracts in the Arcuate Fasciculus (AF) [58,59], but also are language-related regions [49–51,60–64]. The AF is thought to connect Broca's area to Wernicke's area (BA 22/39/40) [65,66], but the temporal projections of the AF could also reach the STG (BA 22) and the MTG (BA 21). These latter regions have projections that reach the premotor cortex (BA 6) and the middle frontal gyrus (BA 9 and BA 10) [58,59]. For the contralateral hemisphere to the stimulation, communication with the stimulated area could be achieved through the corpus callosum and its projections to those areas [67]. Therefore, given those known structural connections it is not surprising that outgoing information from the Broca's area also flowed into ipsilateral and contralateral regions for BA 6, BA 9, BA 10, BA 21 and BA22/39/40. Wernicke's area (BA 39/40) is involved in language comprehension [61], the

Biomedical Optics EXPRESS

STG (BA 22) is part of Wernicke's area and is related with prosody comprehension [63], the premotor cortex (BA 6) is related with maintenance and execution of speech [49,50], the DLPFC (BA 9) is related with speech planning [51] and frontopolar area (BA 10) is related with memory [62,64]. Further support for the observed patterns of information flow comes from the perspective of the topological properties of brain networks [17]. Highly connected regions, known as network hubs, possess the highest levels of neuronal activity [68,69]. Broca's area and its contralateral hemisphere homologue are known hubs [70], so it is reasonable to hypothesize that they could become sources of net information outflow due to an increase in firing rates [71] induced by anodal tDCS.

Another noteworthy point is that during High Current tDCS the MTG (BA 21), identified by the pink circle in Fig. 4, had significant changes in information influx identified from pairwise t-tests in dPTE compared to the Before tDCS condition. Table 1 shows that the MTG had increased information flow from the left Broca's area while it also had information efflux itself towards other areas (Ipsilateral hemisphere: BA6, 9, 10, 22/39/40; Contralateral Hemisphere: BA 6, 9, 10, 22/39/40). Therefore the MTG became a secondary information transfer connector, which is supported from previous literature [72].

Finally, Fig. 4 suggests that information flow patterns appearing during Low Current tDCS are qualitatively similar to those appearing during the High Current tDCS and After High Current tDCS sessions. However, when it comes to the question of whether Low Current tDCS is predictive of the information flow pattern changes between Brodmann areas created by higher currents, Tables 1 and 2 suggest that it is not. Nevertheless, some interesting frequency band specific resemblances in information flow patterns between stimulation sessions were noted and are discussed below.

4.2 Information flow in the endothelial frequency band (0.003-0.02 Hz)

TDCS created greater changes in outgoing information on the left hemisphere, over and around the stimulation area. As shown in Fig. 4, hot spots before tDCS in the left DLPFC and Somatosensory Association Cortex, which are part of the DMN [48], disappeared after stimulation even for Low Current tDCS. At the same time with stimulation, outgoing information hot spots appeared over key language areas such as Broca's area, STG and MTG and persisted during the After tDCS session. The fact that information flowed out of these hotspots towards other cortical regions including Wernicke's area, DPFLC and premotor area is not surprising since these regions are known to be involved in pathways that activate for several speech-related tasks, such as picture naming [73] and overt speech production [74].

Hemodynamic fluctuation changes in the endothelial frequency band, reflect endothelial cell activity mediated by the release of nitric oxide (NO), a vasodilator [25,27,75]. It is possible that tDCS could increase NO production so as to increase brain perfusion [76]. However, the fact that there were significant increases in information efflux in the contralateral hemisphere also (Fig. 7), indicates that hemodynamic changes in this frequency band were at least in part related to changes in neuronal connectivity. Nevertheless, the largest increase in information efflux was observed locally, in the vicinity of the stimulation area. This local dependence is unlikely to be related to tDCS-induced heating at the current intensities used and were well below the known limits of current induced heating during tDCS [77,78]. A NO-based mechanism of endothelial response to stimulation would be consistent with the findings summarized in Table 3, where the flow information patterns during Low Current tDCS were similar to the After High Current tDCS session, whereas higher dPTE values were observed during the High Current tDCS session. A positive relationship between the amount of NO release with the current density of tDCS has been previously reported [76].

In addition, in Table 3, Wernicke's area became an information receiver not only during High Current tDCS but also during Low Current tDCS and After High Current tDCS. Since Broca's area and Wernicke's area are the two main language areas [79], we hypothesize that

Biomedical Optics EXPRESS

the baseline connection between them is stronger compared to other cortical regions, which is why information flow between them was seen even during the Low Current tDCS session. Furthermore, in this frequency band and during Low Current tDCS the same Brodmann areas received increased information flow as in the After High Current tDCS session (Table 3).

4.3 Information flow in the neurogenic frequency band (0.02-0.04 Hz)

Interestingly, tDCS created stronger changes in outgoing information on the non-stimulated right hemisphere, over and around the contralateral stimulation area. As shown in Fig. 8, the hot spots before stimulation occurred in right dorsolateral prefrontal cortex regions, which are part of the DMN [48]. After stimulation, these hot spots disappeared and new ones appeared over key language areas: Broca's area, STG and MTG, which became information efflux spots towards other cortical regions including Wernicke's area, DPFLC, the frontopolar and premotor areas. These latter cortical regions are known to activate in speech-related tasks, such as picture naming [73].

Hemodynamic oscillations in the neurogenic frequency band are attributed to intrinsic nervous activity [28]. Since tDCS could induce a sustainable response in the form of LTP-like plasticity within and across structurally connected brain regions [54,55], it is possible that the right Broca's homologue and related areas became information efflux hot spots due to the increased neuronal activity induced by the pre-existing connections with the left Broca's area. An LTP-like plasticity mechanism of neurogenic response to stimulation would be consistent with the findings summarized in Table 4, where the flow information patterns during Low Current tDCS were similar to the After High Current tDCS session. These results are in contrast to those listed in Table 3 for the endothelial frequency band, where the Low Current tDCS sessions shared the same increased information influx regions as the After High Current tDCS session. An LTP-like plasticity hypothesis is also consistent with findings in the literature [1], indicating that during a 1 mA 5 min application of tDCS over the motor cortex, there was a significant increase in motor-evoked potential amplitude representing the excitability of the motor system, and this effect still persisted after tDCS.

4.4 Information flow in the myogenic frequency band (0.04-0.15 Hz)

TDCS appeared to have little effect on the information flow patterns of the myogenic frequency band, as there was no significant difference in dPTE for hot spots between stimulation sessions. As shown in Fig. 9, hot spots were located in the frontopolar areas (BA10) that are related to prospective memory. The left BA 10 is involved in verbal prospective memory, while right BA 10 is involved in visual-spatial prospective memory [64]. The non-dependence of information flow patterns on tDCS may be due to Mayer waves existing in the same frequency range (~0.1 Hz) from the supraorbital artery located on top of these Brodmann areas [54] and therefore may not be directly related to their function.

4.5 dPTE versus functional connectivity metrics

Finally, it should be clarified that the net information flow change defined by the dPTE metric does not represent one-way information flow, but rather net directional flow, and dPTE is also known to be independent of steady-state connectivity strength [17]. We have recently reported resting-state functional connectivity pattern changes induced by tDCS for the same subjects and fNIRS data [80]. The main finding in that work was that anodal stimulation enhanced the connectivity strength with cortical areas in the immediate vicinity of the stimulated Broca's area, while suppressing longer distance connections. In this work it was found that the number of dPTE source channels over BAs involved in language processing did not change significantly between stimulation conditions, implying that the physical size of dPTE sources did not increase measurably with this fNIRS setup. Nevertheless dPTE values did increase significantly relative to baseline for these channels for all stimulation conditions, even for cortical locations remote to the stimulated area. Comparison between results from

Biomedical Optics EXPRESS

prior analyses and this work confirms that there is no resemblance between changes in information flow patterns and changes in connectivity strength induced by tDCS.

4.6 Limitation of the study and future work

Several potential limitations in the study should be noted. Firstly, only two female subjects were recruited. However, we have found only very minor differences in connectivity pattern changes between males and females in our previous work [80] and no observable differences in dPTE patterns in this work. A larger number of subjects would be needed to demonstrate with statistical significance any possible gender-specific differences on language network modifications induced by tDCS. To our knowledge there are no studies of this kind in current literature although there is evidence of gender-specific differences in language processing networks, e.g [81,82]. Secondly, the participants were not measured twice, so data obtained in this study could not determine the test-retest reliability of dPTE patterns, which needs to be studied in future work. Thirdly, there exist several ways to remove global interference due to the scalp and skull hemodynamics in addition to the PCA method used in this work. Superficial hemodynamics removal methods include (i) adding short-separation channels and using them to regress extra-cerebral effects [83-87], (ii) calculating the mean signal over all channels and using the mean as the superficial regressor [88, 89], or (iii) combining both of these approaches [90]. In addition, data-driven approaches other than PCA [39, 40], such as ICA [91, 92], can be used for this removal. It is unknown which approach is optimal in this regard [93]. In this study, we chose PCA as a method to regress the extra-cerebral effects. A quantitative comparison using different methods is needed in future studies in order to optimally remove the extra-cerebral signals from fNIRS measurements.

5. Conclusion

This study demonstrates the feasibility of using resting-state fNIRS to map changes in the direction of information flow induced by tDCS in the language-processing cortical networks of healthy subjects. While dPTE analysis showed that language-processing cortical regions in both hemispheres became sources of outgoing information flow after tDCS when the entire fNIRS signal was considered, specific differences in those patterns were seen when the detected hemodynamic fluctuations were studied in distinct frequency bands. We found that tDCS induced higher changes in outgoing information in the vicinity of the stimulated Broca's area for the endothelial frequency band, although significant information efflux was also seen for the contralateral Broca's homologue area. We hypothesized that a contributing factor to the higher information outflow over the stimulated area was the known correlation between tDCS current density and NO release levels in brain tissue. On the other hand, for the neurogenic frequency band higher changes in outgoing information were induced in the vicinity of the right Broca's homologue, in the contralateral hemisphere to the stimulation location. We hypothesized that this increase in outgoing information was related to tDCS effects on LTP-like plasticity in established neuronal connections for the language-processing network. Finally, the Before tDCS patterns seen in the myogenic frequency band persisted during all stimulation sessions, which likely relates to Mayer waves created by arterial blood vessels on the cortical surface. It also worthwhile pointing out the potential utility of Low Current tDCS as a method to create short-lived, transient changes in information flow patterns that are qualitatively similar to the longer lasting patterns seen during High Current tDCS. This similarity could enable using Low Current tDCS as a way to form a rapid, qualitative preview of possible information flow patterns seen during a therapeutic tDCS intervention. The methods described in this work for identifying changes in hemodynamic frequency-specific patterns of information flow induced by tDCS could complement and help enhance data analyses in future studies of stimulation-based therapeutic interventions.

Biomedical Optics EXPRESS

Appendix

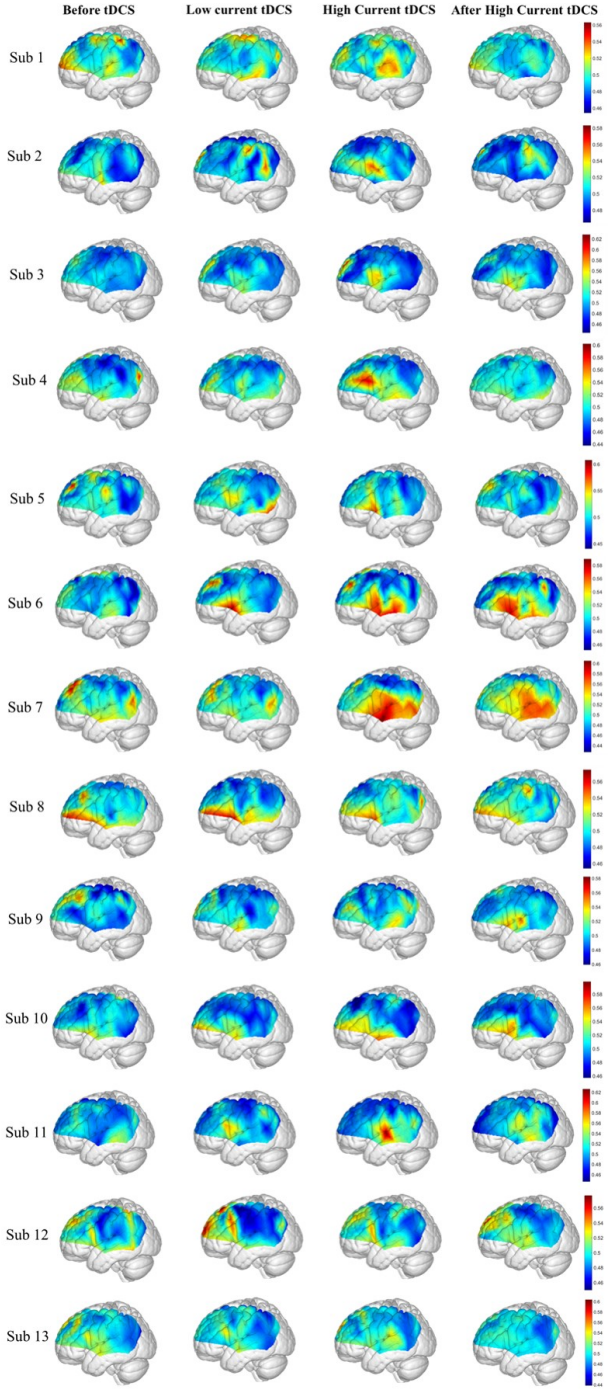

Fig. 10. Mean dPTE for each channel of entire frequency band displayed as a color-coded map viewed from left for the four stimulation sessions of 13 subjects: Before tDCS [first column], Low Current tDCS [second column], High Current tDCS [third column] and After High Current tDCS [fourth column]. Hot (yellow – red) and cold (blue – green) colors indicate information outflow and inflow, respectively.

Biomedical Optics EXPRESS

Disclosures

The authors declare that there are no conflicts of interest related to this article.

References

1. M. A. Nitsche and W. Paulus, "Excitability changes induced in the human motor cortex by weak transcranial direct current stimulation," J. Physiol. **527**(3), 633–639 (2000).
2. M. A. Nitsche and W. Paulus, "Sustained excitability elevations induced by transcranial DC motor cortex stimulation in humans," Neurology **57**(10), 1899–1901 (2001).
3. F. Fregni, P. S. Boggio, M. Nitsche, F. Bermpohl, A. Antal, E. Feredoes, M. A. Marcolin, S. P. Rigonatti, M. T. Silva, W. Paulus, and A. Pascual-Leone, "Anodal transcranial direct current stimulation of prefrontal cortex enhances working memory," Exp. Brain Res. **166**(1), 23–30 (2005).
4. T. Z. Kincses, A. Antal, M. A. Nitsche, O. Bártfai, and W. Paulus, "Facilitation of probabilistic classification learning by transcranial direct current stimulation of the prefrontal cortex in the human," Neuropsychologia **42**(1), 113–117 (2004).
5. R. Sparing, M. Dafotakis, I. G. Meister, N. Thirugnanasambandam, and G. R. Fink, "Enhancing language performance with non-invasive brain stimulation-a transcranial direct current stimulation study in healthy humans," Neuropsychologia **46**(1), 261–268 (2008).
6. B. Elsner, J. Kugler, M. Pohl, and J. Mehrholz, "Transcranial direct current stimulation (tDCS) for improving function and activities of daily living in patients after stroke," Cochrane Database Syst. Rev. **11**(11), CD009645 (2013).
7. J. M. Baker, C. Rorden, and J. Fridriksson, "Using transcranial direct-current stimulation to treat stroke patients with aphasia," Stroke **41**(6), 1229–1236 (2010).
8. J. Fridriksson, J. D. Richardson, J. M. Baker, and C. Rorden, "Transcranial direct current stimulation improves naming reaction time in fluent aphasia: a double-blind, sham-controlled study," Stroke **42**(3), 819–821 (2011).
9. V. Fiori, M. Coccia, C. V. Marinelli, V. Vecchi, S. Bonifazi, M. G. Ceravolo, L. Provinciali, F. Tomaiuolo, and P. Marangolo, "Transcranial direct current stimulation improves word retrieval in healthy and nonfluent aphasic subjects," J. Cogn. Neurosci. **23**(9), 2309–2323 (2011).
10. A. Flöel, N. Rösser, O. Michka, S. Knecht, and C. Breitenstein, "Noninvasive brain stimulation improves language learning," J. Cogn. Neurosci. **20**(8), 1415–1422 (2008).
11. R. Holland, A. P. Leff, O. Josephs, J. M. Galea, M. Desikan, C. J. Price, J. C. Rothwell, and J. Crinion, "Speech facilitation by left inferior frontal cortex stimulation," Curr. Biol. **21**(16), 1403–1407 (2011).
12. M. Meinzer, D. Antonenko, R. Lindenberg, S. Hetzer, L. Ulm, K. Avirame, T. Flaisch, and A. Flöel, "Electrical brain stimulation improves cognitive performance by modulating functional connectivity and task-specific activation," J. Neurosci. **32**(5), 1859–1866 (2012).
13. P. Marangolo, V. Fiori, U. Sabatini, G. De Pasquale, C. Razzano, C. Caltagirone, and T. Gili, "Bilateral transcranial direct current stimulation language treatment enhances functional connectivity in the left hemisphere: preliminary data from aphasia," J. Cogn. Neurosci. **28**(5), 724–738 (2016).
14. R. Holland, A. P. Leff, W. D. Penny, J. C. Rothwell, and J. Crinion, "Modulation of frontal effective connectivity during speech," Neuroimage **140**, 126–133 (2016).
15. M. Lobier, F. Siebenhühner, S. Palva, and J. M. Palva, "Phase transfer entropy: a novel phase-based measure for directed connectivity in networks coupled by oscillatory interactions," Neuroimage **85**(Pt 2), 853–872 (2014).
16. M. Wibral, B. Rahm, M. Rieder, M. Lindner, R. Vicente, and J. Kaiser, "Transfer entropy in magnetoencephalographic data: quantifying information flow in cortical and cerebellar networks," Prog. Biophys. Mol. Biol. **105**(1-2), 80–97 (2011).
17. A. Hillebrand, P. Tewarie, E. van Dellen, M. Yu, E. W. Carbo, L. Douw, A. A. Gouw, E. C. van Straaten, and C. J. Stam, "Direction of information flow in large-scale resting-state networks is frequency-dependent," Proc. Natl. Acad. Sci. U.S.A. **113**(14), 3867–3872 (2016).
18. M. A. Franceschini, S. Fantini, J. H. Thompson, J. P. Culver, and D. A. Boas, "Hemodynamic evoked response of the sensorimotor cortex measured noninvasively with near-infrared optical imaging," Psychophysiology **40**(4), 548–560 (2003).
19. B. Khan, T. Hodics, N. Hervey, G. Kondraske, A. M. Stowe, and G. Alexandrakis, "Functional near-infrared spectroscopy maps cortical plasticity underlying altered motor performance induced by transcranial direct current stimulation," J. Biomed. Opt. **18**(11), 116003 (2013).
20. A. Villringer, "Understanding functional neuroimaging methods based on neurovascular coupling," in *Optical Imaging of Brain Function and Metabolism 2* (Springer, 1997), pp. 177–193.
21. B. M. Bosch, A. Bringard, G. Ferretti, S. Schwartz, and K. Iglói, "Effect of cerebral vasomotion during physical exercise on associative memory, a near-infrared spectroscopy study," Neurophotonics **4**(4), 041404 (2017).
22. C. Aalkjær, D. Boedtkjer, and V. Matchkov, "Vasomotion - what is currently thought?" Acta Physiol. (Oxf.) **202**(3), 253–269 (2011).
23. T. Sakurai and N. Terui, "Effects of sympathetically induced vasomotion on tissue-capillary fluid exchange," Am. J. Physiol. Heart Circ. Physiol. **291**(4), H1761–H1767 (2006).
24. H. Nilsson and C. Aalkjaer, "Vasomotion: mechanisms and physiological importance," Mol. Interv. **3**(2), 79–89, 51 (2003).

Biomedical Optics EXPRESS

25. A. Stefanovska, "Coupled oscillators. Complex but not complicated cardiovascular and brain interactions," IEEE Eng. Med. Biol. Mag. **26**(6), 25–29 (2007).
26. H. Obrig, M. Neufang, R. Wenzel, M. Kohl, J. Steinbrink, K. Einhäupl, and A. Villringer, "Spontaneous low frequency oscillations of cerebral hemodynamics and metabolism in human adults," Neuroimage **12**(6), 623–639 (2000).
27. H. D. Kvernmo, A. Stefanovska, K. A. Kirkebøen, and K. Kvernebo, "Oscillations in the human cutaneous blood perfusion signal modified by endothelium-dependent and endothelium-independent vasodilators," Microvasc. Res. **57**(3), 298–309 (1999).
28. R. Zhang, J. H. Zuckerman, K. Iwasaki, T. E. Wilson, C. G. Crandall, and B. D. Levine, "Autonomic neural control of dynamic cerebral autoregulation in humans," Circulation **106**(14), 1814–1820 (2002).
29. A. C. Merzagora, G. Foffani, I. Panyavin, L. Mordillo-Mateos, J. Aguilar, B. Onaral, and A. Oliviero, "Prefrontal hemodynamic changes produced by anodal direct current stimulation," Neuroimage **49**(3), 2304–2310 (2010).
30. F. Irani, S. M. Platek, S. Bunce, A. C. Ruocco, and D. Chute, "Functional near infrared spectroscopy (fNIRS): an emerging neuroimaging technology with important applications for the study of brain disorders," Clin. Neuropsychol. **21**(1), 9–37 (2007).
31. J. C. Ye, S. Tak, K. E. Jang, J. Jung, and J. Jang, "NIRS-SPM: statistical parametric mapping for near-infrared spectroscopy," Neuroimage **44**(2), 428–447 (2009).
32. F. Tian, F. A. Kozel, A. Yennu, P. E. Croarkin, S. M. McClintock, K. S. Mapes, M. M. Husain, and H. Liu, "Test-retest assessment of cortical activation induced by repetitive transcranial magnetic stimulation with brain atlas-guided optical topography," J. Biomed. Opt. **17**(11), 116020 (2012).
33. W. D. Penny, K. J. Friston, J. T. Ashburner, S. J. Kiebel, and T. E. Nichols, *Statistical Parametric Mapping: the Analysis of Functional Brain Images* (Elsevier, 2011).
34. G. H. Klem, H. O. Lüders, H. H. Jasper, and C. Elger, "The ten-twenty electrode system of the International Federation," Electroencephalogr. Clin. Neurophysiol. Suppl. **52**, 3–6 (1999).
35. A. Antal, R. Polania, C. Schmidt-Samoa, P. Dechent, and W. Paulus, "Transcranial direct current stimulation over the primary motor cortex during fMRI," Neuroimage **55**(2), 590–596 (2011).
36. B. Khan, T. Hodics, N. Hervey, G. Kondraske, A. Stowe, and G. Alexandrakis, "Enhancing motor performance improvement by personalizing non-invasive cortical stimulation with concurrent functional near-infrared spectroscopy and multi-modal motor measurements," in *SPIE BiOS*, (International Society for Optics and Photonics, 2015), 93051A.
37. T. J. Huppert, S. G. Diamond, M. A. Franceschini, and D. A. Boas, "HomER: a review of time-series analysis methods for near-infrared spectroscopy of the brain," Appl. Opt. **48**(10), D280–D298 (2009).
38. Z. Zhang and R. Khatami, "Predominant endothelial vasomotor activity during human sleep: a near-infrared spectroscopy study," Eur. J. Neurosci. **40**(9), 3396–3404 (2014).
39. Y. Zhang, D. H. Brooks, M. A. Franceschini, and D. A. Boas, "Eigenvector-based spatial filtering for reduction of physiological interference in diffuse optical imaging," J. Biomed. Opt. **10**(1), 011014 (2005).
40. X. Zhang, J. A. Noah, and J. Hirsch, "Separation of the global and local components in functional near-infrared spectroscopy signals using principal component spatial filtering," Neurophotonics **3**(1), 015004 (2016).
41. J. Cao, B. Khan, N. Hervey, F. Tian, M. R. Delgado, N. J. Clegg, L. Smith, H. Roberts, K. Tulchin-Francis, A. Shierk, L. Shagman, D. MacFarlane, H. Liu, and G. Alexandrakis, "Evaluation of cortical plasticity in children with cerebral palsy undergoing constraint-induced movement therapy based on functional near-infrared spectroscopy," J. Biomed. Opt. **20**(4), 046009 (2015).
42. B. Biswal, F. Z. Yetkin, V. M. Haughton, and J. S. Hyde, "Functional connectivity in the motor cortex of resting human brain using echo-planar MRI," Magn. Reson. Med. **34**(4), 537–541 (1995).
43. X. Cui, S. Bray, and A. L. Reiss, "Functional near infrared spectroscopy (NIRS) signal improvement based on negative correlation between oxygenated and deoxygenated hemoglobin dynamics," Neuroimage **49**(4), 3039–3046 (2010).
44. M. Rosenblum, A. Pikovsky, J. Kurths, C. Schäfer, and P. A. Tass, "Phase synchronization: from theory to data analysis," *Handbook of Biological Physics*, Vol. 4 (Elsevier, 2001), pp. 279–321.
45. M. Staniek and K. Lehnertz, "Symbolic transfer entropy: inferring directionality in biosignals," Biomed. Tech. (Berl.) **54**(6), 323–328 (2009).
46. F. Tian, Z.-J. Lin, and H. Liu, "EasyTopo: A toolbox for rapid diffuse optical topography based on a standard template of brain atlas," in *Proc. of SPIE Vol*, 2013), 85782J.
47. M. Xia, J. Wang, and Y. He, "BrainNet Viewer: a network visualization tool for human brain connectomics," PLoS One **8**(7), e68910 (2013).
48. M. D. Greicius, B. Krasnow, A. L. Reiss, and V. Menon, "Functional connectivity in the resting brain: a network analysis of the default mode hypothesis," Proc. Natl. Acad. Sci. U.S.A. **100**(1), 253–258 (2003).
49. M. Meinzer, C. Breitenstein, U. Westerhoff, J. Sommer, N. Rösser, A. D. Rodriguez, S. Harnish, S. Knecht, and A. Flöel, "Motor cortex preactivation by standing facilitates word retrieval in aphasia," Neurorehabil. Neural Repair **25**(2), 178–187 (2011).
50. M. Meinzer, R. Lindenberg, M. M. Sieg, L. Nachtigall, L. Ulm, and A. Flöel, "Transcranial direct current stimulation of the primary motor cortex improves word-retrieval in older adults," Front. Aging Neurosci. **6**, 253 (2014).

Biomedical Optics EXPRESS

51. A. Fertonani, S. Rosini, M. Cotelli, P. M. Rossini, and C. Miniussi, "Naming facilitation induced by transcranial direct current stimulation," Behav. Brain Res. **208**(2), 311–318 (2010).
52. M. Quigley, D. Cordes, P. Turski, C. Moritz, V. Haughton, R. Seth, and M. E. Meyerand, "Role of the corpus callosum in functional connectivity," AJNR Am. J. Neuroradiol. **24**(2), 208–212 (2003).
53. T. J. Teyler and P. DiScenna, "Long-term potentiation," Annu. Rev. Neurosci. **10**(1), 131–161 (1987).
54. S. J. Pelletier and F. Cicchetti, "Cellular and molecular mechanisms of action of transcranial direct current stimulation: evidence from in vitro and in vivo models," Int. J. Neuropsychopharmacol. **18**(2), pyu047 (2015).
55. J. P. Brasil-Neto, "Learning, memory, and transcranial direct current stimulation," Front. Psychiatry **3**, 80 (2012).
56. C. Repper-Day, "Mapping dynamic brain connectivity using EEG, TMS, and Transfer Entropy," (University of Manchester, 2017).
57. C. J. Bajada, H. A. Haroon, H. Azadbakht, G. J. Parker, M. A. L. Ralph, and L. L. Cloutman, "The tract terminations in the temporal lobe: Their location and associated functions," Cortex **97**, 277–290 (2016).
58. A. D. Friederici, "Pathways to language: fiber tracts in the human brain," Trends Cogn. Sci. **13**(4), 175–181 (2009).
59. J. K. Rilling, M. F. Glasser, T. M. Preuss, X. Ma, T. Zhao, X. Hu, and T. E. Behrens, "The evolution of the arcuate fasciculus revealed with comparative DTI," Nat. Neurosci. **11**(4), 426–428 (2008).
60. A. S. Dick, S. Goldin-Meadow, U. Hasson, J. I. Skipper, and S. L. Small, "Co-speech gestures influence neural activity in brain regions associated with processing semantic information," Hum. Brain Mapp. **30**(11), 3509–3526 (2009).
61. N. F. Dronkers, D. P. Wilkins, R. D. Van Valin, Jr., B. B. Redfern, and J. J. Jaeger, "Lesion analysis of the brain areas involved in language comprehension," Cognition **92**(1-2), 145–177 (2004).
62. E. Tulving, S. Kapur, H. J. Markowitsch, F. I. Craik, R. Habib, and S. Houle, "Neuroanatomical correlates of retrieval in episodic memory: auditory sentence recognition," Proc. Natl. Acad. Sci. U.S.A. **91**(6), 2012–2015 (1994).
63. D. Wildgruber, A. Riecker, I. Hertrich, M. Erb, W. Grodd, T. Ethofer, and H. Ackermann, "Identification of emotional intonation evaluated by fMRI," Neuroimage **24**(4), 1233–1241 (2005).
64. A. Costa, M. Oliveri, F. Barban, S. Bonnì, G. Koch, C. Caltagirone, and G. A. Carlesimo, "The right frontopolar cortex is involved in visual-spatial prospective memory," PLoS One **8**(2), e56039 (2013).
65. M. Catani, D. K. Jones, and D. H. ffytche, "Perisylvian language networks of the human brain," Ann. Neurol. **57**(1), 8–16 (2005).
66. M. Catani and M. T. de Schotten, *Atlas of human brain connections* (Oxford University Press, 2012).
67. A. De Benedictis, L. Petit, M. Descoteaux, C. E. Marras, M. Barbareschi, F. Corsini, M. Dallabona, F. Chioffi, and S. Sarubbo, "New insights in the homotopic and heterotopic connectivity of the frontal portion of the human corpus callosum revealed by microdissection and diffusion tractography," Hum. Brain Mapp. **37**(12), 4718–4735 (2016).
68. J.-Y. Moon, U. Lee, S. Blain-Moraes, and G. A. Mashour, "General relationship of global topology, local dynamics, and directionality in large-scale brain networks," PLOS Comput. Biol. **11**(4), e1004225 (2015).
69. W. de Haan, K. Mott, E. C. van Straaten, P. Scheltens, and C. J. Stam, "Activity dependent degeneration explains hub vulnerability in Alzheimer's disease," PLOS Comput. Biol. **8**(8), e1002582 (2012).
70. E. H. Nijhuis, A. M. van Cappellen van Walsum, and D. G. Norris, "Topographic hub maps of the human structural neocortical network," PLoS One **8**(6), e65511 (2013).
71. T. Akam and D. M. Kullmann, "Oscillations and filtering networks support flexible routing of information," Neuron **67**(2), 308–320 (2010).
72. E. Bullmore and O. Sporns, "The economy of brain network organization," Nat. Rev. Neurosci. **13**(5), 336–349 (2012).
73. S. Kiran, E. L. Meier, K. J. Kapse, and P. A. Glynn, "Changes in task-based effective connectivity in language networks following rehabilitation in post-stroke patients with aphasia," Front. Hum. Neurosci. **9**, 316 (2015).
74. S. B. Eickhoff, S. Heim, K. Zilles, and K. Amunts, "A systems perspective on the effective connectivity of overt speech production," Philosophical Transactions of the Royal Society of London A: Mathematical," Physical and Engineering Sciences **367**(1896), 2399–2421 (2009).
75. U. Förstermann and W. C. Sessa, "Nitric oxide synthases: regulation and function," Eur. Heart J. **33**(7), 829–837, 837a–837d (2012).
76. D. P. Trivedi, K. J. Hallock, and P. R. Bergethon, "Electric fields caused by blood flow modulate vascular endothelial electrophysiology and nitric oxide production," Bioelectromagnetics **34**(1), 22–30 (2013).
77. M. Bikson, A. Datta, and M. Elwassif, "Establishing safety limits for transcranial direct current stimulation," Clin. Neurophysiol. **120**(6), 1033–1034 (2009).
78. M. A. Nitsche, D. Liebetanz, N. Lang, A. Antal, F. Tergau, and W. Paulus, "Safety criteria for transcranial direct current stimulation (tDCS) in humans," Clin. Neurophysiol. **114**(11), 2220–2222, author reply 2222–2223 (2003).
79. J. R. Binder, J. A. Frost, T. A. Hammeke, R. W. Cox, S. M. Rao, and T. Prieto, "Human brain language areas identified by functional magnetic resonance imaging," J. Neurosci. **17**(1), 353–362 (1997).
80. J. Cao and H. Liu, "Modulating the resting-state functional connectivity patterns of language processing areas in the human brain with anodal transcranial direct current stimulation applied over the Broca's area," Neurophotonics **5**(2), 025002 (2018).

Biomedical Optics EXPRESS

81. V. Beaucousin, L. Zago, P.-Y. Hervé, K. Strelnikov, F. Crivello, B. Mazoyer, and N. Tzourio-Mazoyer, "Sex-dependent modulation of activity in the neural networks engaged during emotional speech comprehension," Brain Res. **1390**, 108–117 (2011).
82. D. Zilles, M. Lewandowski, H. Vieker, I. Henseler, E. Diekhof, T. Melcher, M. Keil, and O. Gruber, "Gender differences in verbal and visuospatial working memory performance and networks," Neuropsychobiology **73**(1), 52–63 (2016).
83. T. Funane, H. Atsumori, T. Katura, A. N. Obata, H. Sato, Y. Tanikawa, E. Okada, and M. Kiguchi, "Quantitative evaluation of deep and shallow tissue layers' contribution to fNIRS signal using multi-distance optodes and independent component analysis," Neuroimage **85**(Pt 1), 150–165 (2014).
84. T. Funane, H. Sato, N. Yahata, R. Takizawa, Y. Nishimura, A. Kinoshita, T. Katura, H. Atsumori, M. Fukuda, K. Kasai, H. Koizumi, and M. Kiguchi, "Concurrent fNIRS-fMRI measurement to validate a method for separating deep and shallow fNIRS signals by using multidistance optodes," Neurophotonics **2**(1), 015003 (2015).
85. R. B. Saager, N. L. Telleri, and A. J. Berger, "Two-detector Corrected Near Infrared Spectroscopy (C-NIRS) detects hemodynamic activation responses more robustly than single-detector NIRS," Neuroimage **55**(4), 1679–1685 (2011).
86. L. Gagnon, M. A. Yücel, D. A. Boas, and R. J. Cooper, "Further improvement in reducing superficial contamination in NIRS using double short separation measurements," Neuroimage **85**(Pt 1), 127–135 (2014).
87. F. Scarpa, S. Brigadoi, S. Cutini, P. Scatturin, M. Zorzi, R. Dell'acqua, and G. Sparacino, "A reference-channel based methodology to improve estimation of event-related hemodynamic response from fNIRS measurements," Neuroimage **72**, 106–119 (2013).
88. G. Pfurtscheller, G. Bauernfeind, S. C. Wriessnegger, and C. Neuper, "Focal frontal (de)oxyhemoglobin responses during simple arithmetic," Int. J. Psychophysiol. **76**(3), 186–192 (2010).
89. G. Bauernfeind, S. C. Wriessnegger, I. Daly, and G. R. Müller-Putz, "Separating heart and brain: on the reduction of physiological noise from multichannel functional near-infrared spectroscopy (fNIRS) signals," J. Neural Eng. **11**(5), 056010 (2014).
90. S. B. Erdoğan, M. A. Yücel, and A. Akın, "Analysis of task-evoked systemic interference in fNIRS measurements: insights from fMRI," Neuroimage **87**, 490–504 (2014).
91. S. Patel, T. Katura, A. Maki, and I. Tachtsidis, "Quantification of systemic interference in optical topography data during frontal lobe and motor cortex activation: an independent component analysis," in *Oxygen Transport to Tissue XXXII* (Springer, 2011), pp. 45–51.
92. N. Hervey, B. Khan, L. Shagman, F. Tian, M. R. Delgado, K. Tulchin-Francis, A. Shierk, H. Roberts, L. Smith, D. Reid, N. J. Clegg, H. Liu, D. MacFarlane, and G. Alexandrakis, "Motion tracking and electromyography-assisted identification of mirror hand contributions to functional near-infrared spectroscopy images acquired during a finger-tapping task performed by children with cerebral palsy," Neurophotonics **1**(2), 025009 (2014).
93. I. Tachtsidis and F. Scholkmann, "False positives and false negatives in functional near-infrared spectroscopy: issues, challenges, and the way forward," Neurophotonics **3**(3), 031405 (2016).